HHS Public Access

Author manuscript

Cell Stem Cell. Author manuscript; available in PMC 2019 April 25.

Published in final edited form as:

Cell Stem Cell. 2018 September 06; 23(3): 370–381.e5. doi:10.1016/j.stem.2018.07.003.

Distinct Bone Marrow Sources of Pleiotrophin Control Hematopoietic Stem Cell Maintenance and Regeneration

Heather A. Himburg[1], **Christina M. Termini**[1], **Lauren Schlüssel**[1], **Jenny Kan**[1], **Michelle Li**[1], **Liman Zhao**[1], **Tiancheng Fang**[1,2], **Joshua P. Sasine**[1,3,6], **Vivian Y. Chang**[4,5,6], and **John P. Chute**[1,6,7,8,*]

[1]Division of Hematology/Oncology, Department of Medicine, University of California, Los Angeles, Los Angeles, CA 90095, USA

[2]Department of Molecular and Medical Pharmacology, University of California, Los Angeles, Los Angeles, CA 90095, USA

[3]Department of Molecular, Cellular and Integrative Physiology, University of California, Los Angeles, Los Angeles, CA 90095, USA

[4]Division of Pediatric Hematology/Oncology, University of California, Los Angeles, Los Angeles, CA 90095, USA

[5]Children's Discovery and Innovation Institute, University of California, Los Angeles, Los Angeles, CA 90095, USA

[6]Jonsson Comprehensive Cancer Center, University of California, Los Angeles, Los Angeles, CA 90095, USA

[7]Broad Stem Cell Research Center, University of California, Los Angeles, Los Angeles, CA 90095, USA

[8]Lead Contact

SUMMARY

Bone marrow (BM) perivascular stromal cells and vascular endothelial cells (ECs) are essential for hematopoietic stem cell (HSC) maintenance, but the roles of distinct niche compartments during HSC regeneration are less understood. Here we show that Leptin receptor-expressing (LepR+) BM stromal cells and ECs dichotomously regulate HSC maintenance and regeneration via secretion of pleiotrophin (PTN). BM stromal cells are the key source of PTN during steady-state hematopoiesis because its deletion from stromal cells, but not hematopoietic cells, osteoblasts, or ECs, depletes the HSC pool. Following myelosuppressive irradiation, PTN expression is increased in bone

*Correspondence: jchute@mednet.ucla.edu.

AUTHOR CONTRIBUTIONS

J.P.C. designed and directed the study. H.A.H., C.M.T., L.S., J.K., M.L., T.F., and J.S. performed the experiments reported in this study. L.Z. performed mouse breeding and mouse experiments. V.C. performed cell culture and flow cytometry experiments. H.A.H. and J.P.C. wrote the manuscript with input from C.M.T., L.S., J.K., M.L., L.Z., T.F., J.P.S., and V.Y.C.

DECLARATION OF INTERESTS

The authors declare no competing interests.

SUPPLEMENTAL INFORMATION

Supplemental Information includes five figures and can be found with this article online at https://doi.org/10.1016/j.stem.2018.07.003.

marrow endothelial cells (BMECs), and PTN^{+} ECs are more frequent in the niche. Moreover, deleting *Ptn* from ECs impairs HSC regeneration whereas *Ptn* deletion from BM stromal cells does not. These findings reveal dichotomous and complementary regulation of HSC maintenance and regeneration by BM stromal cells and ECs.

In Brief

Himburg et al. demonstrate dichotomous regulation of blood stem cell maintenance and regeneration by BM stromal cells and ECs. Utilizing conditional genetic models, the authors show that blood stem cell maintenance requires PTN secretion by BM stromal cells, whereas blood stem cell regeneration requires complementary PTN production by BMECs.

Graphical Abstract

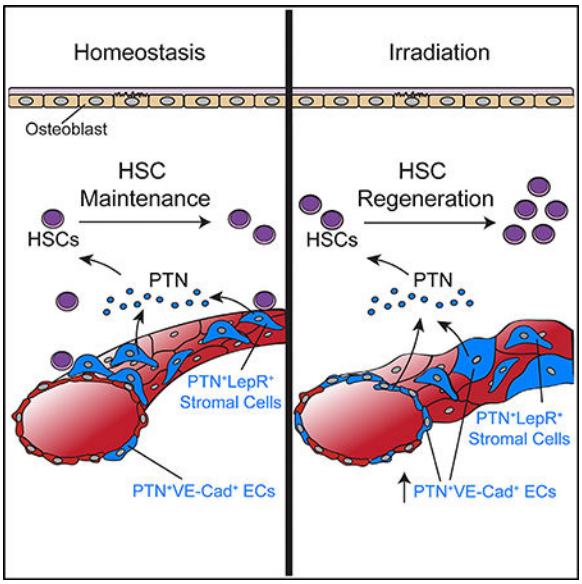

INTRODUCTION

Hematopoietic stem cells (HSCs) reside in vascular niches in which perivascular stromal cells and endothelial cells (ECs) secrete growth factors, including stem cell factor (SCF) and CXCL12, which are essential for maintenance of the HSC pool (Ding et al., 2012; Ding and Morrison, 2013; Greenbaum et al., 2013). Bone marrow (BM) ECs also secrete Jagged-1, which is important for homeostatic hematopoiesis (Poulos et al., 2013). Recent studies suggest that BM arterial blood vessels maintain HSCs in a low reactive oxygen species state, whereas permeable sinusoidal vessels promote HSC activation (Itkin et al., 2016). Furthermore, activation of Notch signaling in ECs increases the number of HSC niches via amplification of CD31^{+} capillaries and platelet-derived growth factor receptor (PDGFR)-β^{+} perivascular cells (Kusumbe et al., 2016). Differential cytokine contributions from perivascular cells have also been demonstrated (Asada et al., 2017). Deletion of *Scf* in LepR^{+} peri-sinusoidal cells reduced HSC numbers whereas *Scf* deletion in NG2^{+} arteriolar perivascular cells did not (Asada et al., 2017). Conversely, deletion of *Cxcl12* from arteriolar

NG2$^+$ perivascular cells decreased HSC numbers, whereas deletion of *Cxcl12* from LepR$^+$ cells had no effect (Asada et al., 2017). Taken together, these studies have characterized the paracrine function of perivascular stromal cells and bone marrow endothelial cells (BMECs) in maintaining HSCs during homeostasis. However, the effects of myeloablation or injury on niche cell regulation of hematopoiesis and the precise mechanisms through which niche cells regulate HSC regeneration after injury remain incompletely understood (Hooper et al., 2009; Salter et al., 2009; Zhou et al., 2015, 2017; Guo et al., 2017; Himburg et al., 2017; Goncalves et al., 2016; Poulos et al., 2013).

We sought to determine the functions of BM niche cells in regulating both HSC maintenance and regeneration by conditionally deleting pleiotrophin *(Ptn),* a heparin-binding growth factor that promotes HSC expansion *in vitro* and HSC regeneration *in vivo,* in a cell-specific manner (Himburg et al., 2010, 2012, 2014). Here we show that deletion of *Ptn* from LepR$^+$ stromal cells impaired HSC maintenance during homeostasis, whereas deletion of *Ptn* from BMECs, osteoblasts, or hematopoietic cells had no effect. Total body irradiation (TBI) enriched for PTN-expressing BMECs in the niche and deletion of *Ptn* from vascular endothelial (VE)-cadherin$^+$ (VE-cad$^+$) ECs markedly impaired HSC regeneration following TBI. Conversely, PTN from LepR$^+$ stromal cells was not required for HSC regeneration to occur. These results demonstrate unpredicted, dichotomous control of HSC maintenance and HSC regeneration by BM stromal cells and ECs via secretion of PTN.

RESULTS

PTN Is Expressed by BM LepR$^+$ Stromal Cells and VE-cad$^+$ ECs

We utilized *Ptn-EGFP* mice to identify cells that express PTN in the adult BM (Michelotti et al., 2016). We observed no expression of PTN by BM CD45$^+$ hematopoietic cells and minimal co-localization of PTN with BM osteopontin$^+$ osteolineage cells (Figures S1A and S1B). Conversely, PTN expression co-localized with BM VE-cad$^+$ ECs and LepR$^+$ stromal cells, which surround BM vessels (Figures 1A–1J). By flow cytometry, a mean of 50% of BM VE-cad$^+$ ECs and 93% of LepR$^+$ stromal cells expressed PTN at baseline (Figures 1K and 1M). Further analysis revealed that 64% of BM CD31$^+$Sca-1$^-$ sinusoidal BMECs (sBMECs) expressed PTN, whereas 29% of CD31$^+$Sca-1$^+$ arteriolar BMECs (aBMECs) expressed PTN (Figures 1L and 1O). A small population of CD31$^+$Endomucin$^+$ ECs also expressed PTN (Figure S1C). Analysis of BM LepR$^+$ stromal cell subsets revealed that 99% of LepR$^+$CXCL12$^+$ stromal cells and 98% of LepR$^+$CXCL12$^-$ stromal cells expressed PTN (Figures 1N and 1O). BM LepR$^+$ PDGFRα$^+$ stromal cells also highly expressed PTN, whereas less than 5% of BM LepR$^-$NG2$^+$ cells expressed PTN (Figures S1D–S1F). Gene expression analysis demonstrated the highest level of *Ptn* expression in BM LepR$^+$ stromal cells and CD31$^+$Sca-1$^-$ sBMECs and no significant evidence of *Ptn* expression in BM CD45$^+$ hematopoietic cells or BM osteoblasts (Figure 1P). Taken together, these analyses demonstrated that PTN is highly expressed by BM LepR$^+$ stromal cell subsets and predominantly expressed by sBMECs.

PTN Is Not Required from Hematopoietic Cells, Osteoblasts, or ECs for HSC Maintenance

To determine the effects of *Ptn* deletion in cells within the hematopoietic system, we generated *Ptn* floxed/floxed mice (*Ptn*$^{fl/fl}$ mice). Of note, adult *Ptn*$^{fl/fl}$ mice were viable and had no evident phenotype at baseline. We crossed *Ptn*$^{fl/fl}$ mice with *Vav1-Cre* mice to delete *Ptn* in all Vav1$^+$ hematopoietic cells (Figure S2A; Ruiz-Herguido et al., 2012). Adult *Vav1-Cre;Ptn*$^{fl/fl}$ mice had normal BM cell counts, colony-forming cell (CFC) content, and percentages of ckit$^+$sca-1$^+$lin$^-$ (KSL) stem/progenitor cells and signaling lymphocyte activation molecule (SLAM)$^+$KSL HSCs (Figures S2B–S2E). Competitive repopulation assays revealed no deficit in HSC function in *Vav1-Cre;Ptn*$^{fl/fl}$ mice compared with control mice (Figure S2F). *Vav1-Cre;Ptn*$^{fl/fl}$ mice also had normal complete blood counts (Figure S2G), spleen weights, and BM differential compared with controls (data not shown). Vav1$^+$ hematopoietic cells are therefore not a required source of PTN for the maintenance of BM HSCs or progenitors.

We next interrogated *Osteocalcin-Cre;Ptn*$^{fl/fl}$ mice (*Ocn-Cre;Ptn*$^{fl/fl}$ mice) to assess the effects of *Ptn* deletion in BM osteocalcin$^+$ osteoblasts (Figure S2A; Raaijmakers et al., 2010). Adult *Ocn-Cre;Ptn*$^{fl/fl}$ mice displayed a normal hematopoietic profile, normal percentages of BM KSL and SLAM$^+$KSL cells, and no HSC functional deficit in competitive repopulation assays (Figures S2B–S2G). These results suggest that BM osteoblasts are not an important source of PTN for maintenance of the HSC or progenitor cell pool.

We crossed *VE-cadherin-Cre* mice (*Ve-cad-Cre*) with *Ptn*$^{fl/fl}$ mice to delete *Ptn* in VE-cad$^+$ ECs (Figure S2A; Alva et al., 2006). *VE-cad-Cre;Ptn*$^{fl/fl}$ mice also displayed no baseline deficit in BM cell counts, complete blood counts, KSL cells or SLAM$^+$ KSL cells and no HSC functional deficit in competitive repopulation assays compared with controls (Figures S2B–S2G). These data suggest that VE-cad$^+$ BMECs are not a required source of PTN for the maintenance of HSCs or progenitor cells during homeostasis.

PTN from LepR$^+$ BM Stromal Cells Is Required for HSC Maintenance

We crossed *LepR-Cre* mice with *Ptn*$^{fl/fl}$ mice to evaluate the effect of *Ptn* deletion in BM stromal cells on hematopoiesis (Figure 2A; Zhou et al., 2017). Adult *LepR-Cre;Ptn*$^{fl/fl}$ mice displayed no significant differences in complete blood counts or spleen weights compared with controls (Figures S3A and S3B). However, *LepR-Cre;Ptn*$^{fl/fl}$ mice contained decreased BM cell counts and decreased BM Mac1$^+$Gr1$^+$ myeloid cells, B220$^+$ B cells, and CD3$^+$ T cells compared with controls (Figure 2B; Figure S3C). Although *LepR-Cre;Ptn*$^{fl/fl}$ mice displayed moderate BM hypocellularity, we noted no differences in BM perilipin$^+$ adipocyte content between *LepR-Cre;Ptn*$^{fl/fl}$ mice and controls (Figure S3D). *LepR-Cre;Ptn*$^{fl/fl}$ mice contained decreased BM CFCs and decreased percentages and numbers of BM KSL cells and SLAM$^+$KSL HSCs compared with controls (Figures 2C–2E; Figure S3E). These results suggested that deletion of *Ptn* from LepR$^+$ stromal cells caused a significant loss of phenotypic HSCs and progenitor cells in homeostasis.

To confirm whether PTN from LepR$^+$ stromal cells was necessary for the maintenance of functional HSCs, we performed competitive repopulation assays using BM cells from *LepR-*

Cre;Ptn$^{fl/fl}$ mice and control donor mice. Syngeneic CD45.1^{+} mice that were competitively transplanted with 2 × 10^{5} CD45.2^{+} BM cells from *LepR-Cre;Ptn*$^{fl/fl}$ mice, along with 2 × 10^{5} competitor CD45.1^{+} BM cells, displayed a significant decrease in donor CD45.2^{+} cell engraftment through 20 weeks post-transplant compared with mice transplanted with the identical dose of BM cells from control mice (Figure 2F). Donor CD45.2^{+} cell contribution to BM CD34^{-}Flt-3^{-}KSL cells, representative of long-term HSCs (LT-HSCs), CD34^{+}Flt-3^{-}KSL short-term HSCs (ST-HSCs), and CD34^{+}Flt-3^{+}KSL multipotent progenitor (MPP) cells was also significantly decreased at 20 weeks in recipients of BM from *LepR-Cre;Ptn*$^{fl/fl}$ mice compared with control mice (Figure 2G; Figure S3F). Secondary competitive transplants confirmed a substantial deficit in LT-HSCs in *LepR-Cre;Ptn*$^{fl/fl}$ mice compared with controls (Figure 2H). Multilineage engraftment of donor myeloid, B cells, and T cells was also decreased in secondary recipients of BM cells from *LepR-Cre;Ptn*$^{fl/fl}$ mice (Figure 2I). Taken together, these results suggested that PTN from BM LepR^{+} stromal cells was necessary for the maintenance of LT-HSCs.

Of note, PTN has been shown to promote angiogenesis in tumor models and at sites of ischemia and inflammation (Christman et al., 2005; Perez-Pinera et al., 2008; Laaroubi et al., 1994; Chauhan et al., 1993). Therefore, we evaluated the BM vasculature of mice bearing deletion of *Ptn* in LepR^{+} and VE-cad^{+} cells compared with control mice. We observed no substantial differences in BM vascular density or BM vessel length between adult *LepR-Cre;Ptn*$^{fl/fl}$ mice, *VE-cad-Cre;Ptn*$^{fl/fl}$ mice, and control mice in a steady state (Figures S3G and S3H). These results suggested that deletion of PTN from LepR^{+} stromal cells or VE-cad^{+} ECs did not alter the BM vasculature in a steady state.

Irradiation Enriches for PTN-Expressing BMECs

Myelosuppressive insults such as chemotherapy or irradiation damage BM niche cell integrity, and niche cell-mediated regulation of hematopoiesis may change following stress (Zhou et al., 2015, 2017; Salter et al., 2009; Lucas et al., 2013). Furthermore, HSC requirements for niche-derived signals may change after injury (Doan et al., 2013). Because PTN is produced primarily by BMECs and stromal cells, we examined the effect of 500 cGy TBI on BM VE-cad^{+} EC and LepR^{+} stromal cell composition and on the expression of PTN in these niche cells over time. Fluorescence microscopic analysis on day +3 following 500 cGy TBI revealed marked disruption of the normal BM vascular architecture coupled with increased PTN co-localization with VE-cad^{+} BMECs and decreased co-localization with LepR^{+} stromal cells (Figures 3A and 3B). On day +10, PTN co-localization with VE-cad^{+} ECs increased further, whereas PTN localization with LepR^{+} stromal cells returned to baseline (Figures 3A and 3B). Flow cytometric analysis revealed that the percentages of both BM VE-cad^{+} ECs and LepR^{+} stromal cells increased, as a fraction of total BM lin^{-} cells, on day +3 following 500 cGy TBI because of the loss of radiosensitive hematopoietic cells (Figures 3C and 3D; Figure S4A). Interestingly, the percentages of BM VE-cad^{+}PTN^{+} ECs increased significantly on day +3 and day +10 following 500 cGy TBI, whereas the percentages of LepR^{+}PTN^{+} stromal cells remained high and unchanged from baseline (Figures 3C and 3D). PTN mean fluorescence intensity (MFI) more than doubled in VE-cad^{+} ECs on day +10 following 500 cGy TBI compared with non-irradiated controls, whereas PTN MFI in LepR^{+} stromal cells decreased in irradiated mice compared with non-irradiated

controls (Figure 3E). Subset analysis revealed that PTN expression also increased in both $CD31^+Sca\text{-}1^-$ sBMECs and $CD31^+Sca\text{-}1^+$ aBMECs on day +3 following TBI (Figure 3F; Figure S4B), whereas PTN expression in $LepR^+$ stromal cell subsets remained unchanged (Figure S4C). *Ptn* gene expression increased 4.2-fold in VE-cad^+ ECs and 7.4-fold in $CD31^+Sca\text{-}1^-$ sBMECs 72 hr following 500 cGy TBI, whereas *Ptn* expression decreased 2.3-fold in BM $LepR^+$ stromal cells compared with non-irradiated mice (Figure 3G). Taken together, these results suggested that TBI induced PTN expression in BMECs and enriched for PTN^+ ECs, particularly in BM sinusoidal vessels. Of note, we observed no change in VE-cad expression in BM VE-cad^+ ECs and a minimal decrease in LepR expression in BM $LepR^+$ cells following 500 cGy TBI (Figure S4D).

Hematologic Recovery after Irradiation Requires PTN from BM Stromal Cells and ECs

To determine the cell-specific requirements for PTN during hematopoietic regeneration, we irradiated *LepR-Cre;*$Ptn^{fl/fl}$ mice and *VE-cad-Cre;*$Ptn^{fl/fl}$ mice with 500 cGy TBI and compared the hematopoietic content of these mice over time with control mice. In non-irradiated mice, PTN levels in the BM of *VE-cad-Cre;*$Ptn^{fl/fl}$ mice and *LepR-Cre;*$Ptn^{fl/fl}$ mice were significantly lower than in control mice, and PTN levels in *LepR-Cre;*$Ptn^{fl/fl}$ mice were also significantly lower than in *VE-cad-Cre;*$Ptn^{fl/fl}$ mice (Figure 4A). On day +1 and day +4 following 500 cGy TBI, BM PTN levels in *LepR-Cre;*$Ptn^{fl/fl}$ mice and *VE-cad-Cre;*$Ptn^{fl/fl}$ mice remained significantly decreased compared with irradiated control mice. However, PTN levels in the BM of *VE-cad-Cre;*$Ptn^{fl/fl}$ mice became significantly lower than in *LepR-Cre;*$Ptn^{fl/fl}$ mice on day +1 and day +4 (Figure 4A). *VE-cad-Cre;*$Ptn^{fl/fl}$ mice displayed significantly decreased peripheral blood (PB) white blood cell (WBC) and neutrophil counts on day +10 and day +14 following 500 cGy TBI as well as decreased PB lymphocytes on day +14 compared with irradiated control mice (Figure 4B; Figure S4E). *VE-cad-Cre;*$Ptn^{fl/fl}$ mice also displayed a significant decrease in BM cell counts, KSL cells, $ckit^+sca\text{-}1^-lin^-$ myeloid progenitor cells and CFCs compared with controls (Figures 4C–4E). Similarly, *LepR-Cre;*$Ptn^{fl/fl}$ mice demonstrated decreased numbers of PB WBCs and neutrophils on day +10 and +14 following 500 cGy TBI and decreased PB lymphocytes on day +14 compared with irradiated control mice (Figure 4B). *LepR-Cre;*$Ptn^{fl/fl}$ mice also contained decreased BM cell counts, KSL cells, and myeloid progenitors on day +10 compared with irradiated controls (Figures 4C–4E). Of note, surface expression of the PTN receptor protein tyrosine phosphatase zeta (PTPζ) concordantly increased on BM KSL cells, myeloid progenitors, and $CD11b^+$ myeloid cells after irradiation, consistent with a facultative role for PTN signaling in hematopoietic stem/progenitor cells (HSPCs) and myeloid cells following irradiation (Figure S4F).

Because deletion of *Ptn* from either VE-cad^+ ECs or $LepR^+$ stromal cells was associated with a deficit in BM KSLs and myeloid progenitors within 10 days following TBI, we tested whether this could alter the survival of irradiated mice. Following 700 cGy TBI, 78% of control mice (7 of 9) remained alive on day +60. In contrast, 22% of *LepR-Cre;*$Ptn^{fl/fl}$ mice (2 of 9) and 22% of *VE-cad-Cre;*$Ptn^{fl/fl}$ mice (2 of 9) remained alive on day +60 ($p = 0.01$ and $p = 0.01$; Figure 4F). Taken together, these results suggested that acute hematologic recovery and survival following irradiation required PTN from BM $LepR^+$ stromal cells and VE-cad^+ ECs.

LT-HSC Regeneration Requires PTN from VE-cad$^+$ ECs

To determine whether LT-HSC regeneration following TBI required PTN from BM LepR$^+$ stromal cells or VE-cad$^+$ ECs, we performed primary and secondary competitive repopulation assays using BM cells collected on day +10 from irradiated *LepR-Cre;Ptn$^{fl/fl}$* mice, *VE-cad-Cre;Ptn$^{fl/fl}$* mice, and controls. Primary recipient mice transplanted with BM cells from *LepR-Cre;Ptn$^{fl/fl}$* mice on day +10 following 500 cGy TBI displayed comparable donor multilineage hematopoietic cell engraftment at 12 weeks as recipient mice transplanted with BM cells from irradiated control mice (Figures 5A and 5B). In contrast, recipient mice transplanted with the identical dose of BM cells from *VE-cad-Cre;Ptn$^{fl/fl}$* mice displayed significantly decreased total CD45.2$^+$ cell engraftment and decreased donor myeloid cells, B cells, and T cells compared with mice transplanted with BM cells from control mice or *LepR-Cre;Ptn$^{fl/fl}$* mice (Figures 5A and 5B). Donor CD45.2$^+$ cell engraftment within BM LT-HSCs, ST-HSCs, and MPP cells was also significantly decreased in recipient mice transplanted with BM cells from *VE-cad-Cre;Ptn$^{fl/fl}$* mice (Figure 5C; Figures S5A and S5B). Secondary competitive transplantation assays demonstrated that irradiated *LepR-Cre;Ptn$^{fl/fl}$* mice displayed no deficit in LT-HSC repopulating capacity compared with irradiated control mice (Figures 5D and 5E). However, irradiated *VE-cad-Cre;Ptn$^{fl/fl}$* mice demonstrated significantly decreased LT-HSC repopulating capacity, as measured by decreased total donor and multilineage engraftment in secondary recipient mice (Figures 5D and 5E). These results suggested that LT-HSC regeneration after TBI required PTN from BM VE-cad$^+$ ECs.

DISCUSSION

Our results suggest that HSC maintenance in steady state is dependent on the secretion of PTN by BM LepR$^+$ stromal cells. Indeed, in steady state, BM LepR$^+$ cells express higher levels of PTN compared with VE-cad$^+$ ECs. Consistent with this, *LepR-Cre;Ptn$^{fl/fl}$* mice displayed significantly lower PTN levels in the BM during homeostasis compared with control mice and *VE-cad-Cre;Ptn$^{fl/fl}$* mice. These results suggest that HSC maintenance requires a threshold level of PTN that is sustained by BM LepR$^+$ stromal cells.

Following TBI, hematologic recovery and survival were both impaired significantly in *LepR-Cre;Ptn$^{fl/fl}$* mice and *VE-cad-Cre;Ptn$^{fl/fl}$* mice. These findings corresponded with significantly decreased levels of PTN protein in the BM of *LepR-Cre;Ptn$^{fl/fl}$* mice and *VE-cad-Cre;Ptn$^{fl/fl}$* mice compared with irradiated, control mice. Yang et al. (2005) showed previously that the majority of radioprotective hematopoietic cells are contained within the CD34$^+$Flt-3$^-$KSL ST-HSC population, whereas LT-HSCs do not contribute significantly to radioprotection, and myeloid progenitors provide radioprotection only at 100-fold higher cell doses (Na Nakorn et al., 2002; Osawa et al., 1996). Both *VE-cad-Cre;Ptn$^{fl/fl}$* mice and *LepR-Cre;Ptn$^{fl/fl}$* mice contained significantly decreased numbers of BM KSL cells and ckit $^+$sca-1$^-$lin$^-$ myeloid progenitor cells on day +10 following 500 cGy TBI. These deficits likely contributed to the decreased survival of *VE-cad-Cre;Ptn$^{fl/fl}$* mice and *LepR-Cre;Ptn$^{fl/fl}$* mice following irradiation. These data suggest that both VE-cad$^+$ ECs and LepR$^+$ stromal cells are essential sources of PTN to support the recovery of radioprotective HSPCs and survival following irradiation.

Following TBI, *VE-cad-Cre;Ptn*$^{fl/fl}$ mice displayed a significant deficit in LT-HSC regeneration, whereas *LepR-Cre;Ptn*$^{fl/fl}$ mice maintained LT-HSC content equivalent to that of irradiated control mice. These results suggest that BM VE-cad$^+$ ECs have a facultative and essential role in supporting LT-HSC regeneration following irradiation via secretion of PTN. Further, these data suggest that BM LepR$^+$PTN$^+$ stromal cells and VE-cad$^+$PTN$^+$ ECs provide dichotomous regulation of HSC maintenance and regeneration. Our analysis of BM niche cell recovery and PTN expression after irradiation provides some insights into potential mechanisms underlying these observations. First, irradiation significantly enriched for BM VE-cad$^+$PTN$^+$ ECs through day +10. TBI also notably increased the expression of PTN by CD31$^+$Sca-1$^-$ sBMECs, which, as part of the BM sinusoidal vascular niche, supports dividing and non-dividing HSC and HSPC trafficking (Acar et al., 2015; Itkin et al., 2016; Chen et al., 2016). The MFI of PTN expression in VE-cad$^+$ ECs and sBMECs also increased after TBI, coupled with an increase in *Ptn* gene expression in these populations, suggesting that irradiation triggered increased transcription and concentration of PTN in BMECs. In keeping with this, Cre-mediated excision of *Ptn* in VE-cad$^+$ ECs caused a substantial decrease in PTN levels in the BM compared with irradiated control mice. In contrast, the percentages of BM PTN$^+$LepR$^+$ stromal cells did not change following irradiation, and *Ptn* gene expression and MFI decreased in LepR$^+$ stromal cells after irradiation. It is difficult to conclude with certainty whether the observed shifts in PTN expression by BM VE-cad$^+$ ECs explain the differences in LT-HSC regeneration between *VE-cad-Cre;Ptn*$^{fl/fl}$ mice and *LepR-Cre;Ptn*$^{fl/fl}$ mice, particularly because irradiation can alter both the identity and recovery of BMECs and stromal cells. Furthermore, irradiation may change the spatial localization of LT-HSCs within the BM microenvironment and alter the requirements for niche sources of paracrine factors such as PTN (Dominici et al., 2009). Heparin binding is a requirement for PTN function (Perez-Pinera et al., 2008; Kinnunen et al., 1996), and cytokine localization with glycosaminoglycans has been shown to promote HSPC maintenance *in vitro* (Gupta et al., 2000). Following irradiation, BMECs may facilitate PTN signaling to HSCs via heparin binding on BMEC surfaces, as shown for BMEC-mediated enhancement of SDF1 binding to CXCR4 on HSPCs (Netelenbos et al., 2003).

Our analysis of *VE-cad-Cre;Ptn*$^{fl/fl}$ mice and *LepR-Cre;Ptn*$^{fl/fl}$ mice following 500 cGy TBI provides the strongest evidence that VE-cad$^+$ ECs are a required source of PTN for LT-HSC regeneration. Multiple independent primary and secondary competitive repopulation assays confirmed that *VE-cad-Cre; Ptn*$^{fl/fl}$ mice contain significantly decreased LT-HSCs on day +10 following irradiation compared with control mice or *LepR-Cre;Ptn*$^{fl/fl}$ mice. Following irradiation, *VE-cad-Cre;Ptn*$^{fl/fl}$ mice also displayed significantly decreased PTN protein levels in the BM compared with *LepR-Cre;Ptn*$^{fl/fl}$ mice, linking *Ptn* deletion in ECs to a deeper physiologic deficit of PTN protein in the BM niche after TBI. These results suggest that a threshold level of PTN may be required for LT-HSC regeneration following irradiation. Because both *VE-cad-Cre;Ptn*$^{fl/fl}$ mice and *LepR-Cre;Ptn*$^{fl/fl}$ mice displayed deficits in myeloid progenitor cell recovery and survival following TBI, this suggests that the sensitivity of myeloid progenitor cells and radioprotective ST-HSCs to PTN deficiency is higher than that of LT-HSCs.

HSC maintenance in homeostasis is dependent on secretion of SCF and CXCL12 by BMECs and perivascular stromal cells (Ding et al., 2012; Ding and Morrison, 2013; Greenbaum et al., 2013). HSC regeneration following irradiation requires recovery of VEGFR2$^+$ BMECs, and recent studies have suggested that EC-derived Jagged 1 and Jagged 2 may be required for hematopoietic regeneration following myelosuppression (Guo et al., 2017; Hooper et al., 2009; Poulos et al., 2013). However, it remains poorly understood whether the required roles of specific niche cells in HSC maintenance are also essential for HSC regeneration and whether specific niche-derived mechanisms that support HSC maintenance are also required for HSC regeneration. These questions have important clinical implications because HSC regeneration is fundamental to hematologic recovery in patients receiving myelosuppressive chemo- and radiotherapy as well as recipients of myeloablative hematopoietic cell transplantation. Recently, Zhou et al. (2017) showed that BM adipocytes facultatively produce SCF in mice following irradiation and that adipocytes and LepR$^+$ stromal cells are essential sources of SCF for HSC regeneration. Here, via interrogation of the paracrine factor PTN, we demonstrate that BM LepR$^+$ stromal cells are essential for HSC maintenance and that VE-cad$^+$ ECs are required for HSC regeneration. These results reveal dichotomous and complementary regulation of HSC fate by BM LepR$^+$ stromal cells and VE-cad$^+$ ECs, which changes following injury. Further, we have discovered that irradiation specifically enriches for BM PTN$^+$ VE-cad$^+$ ECs and PTN$^+$CD31$^+$Sca-1$^-$ sinusoidal ECs in the niche, providing the anatomic basis for the enhanced contribution of BMECs to HSC regeneration following injury. Finally, prior studies have suggested that the dosage of hematopoietic cytokines may be an important factor in regulating HSPC self-renewal and expansion (Cashman and Eaves, 1999; Zandstra et al., 1997). Here we show that LT-HSCs and radioprotective hematopoietic progenitor cells display differential sensitivities to PTN deficiency in the niche following irradiation. This suggests that PTN dosage is important for both LT-HSC regeneration and survival following myelosuppression.

STAR⋆METHODS

CONTACT FOR REAGENT AND RESOURCE SHARING

Further information and requests for resources and reagents should be directed to, and will be fulfilled by, the Lead Contact, John P. Chute M.D. (jchute@mednet.ucla.edu).

EXPERIMENTAL MODEL AND SUBJECT DETAILS

Mice—All animal procedures were performed in accordance with animal use protocol UCLA2014–021-13G, approved by the UCLA Animal Care and Use Committee. All mice were maintained in the UCLA Radiation Oncology vivarium, which is a barrier facility specifically designed for the care of mice following radiation treatment. Experimental mice were separated by sex and housed 4–5 mice per cage in low-noise Optimice Hepa-filtered ventilated cage racks (Animal Care Systems Inc, Centennial Colorado). All mice were healthy and immune competent prior to studies the described. An ear punch or tail snip tissue biopsy was performed to obtain tissue for genotyping when the mice were weaned. Genotyping was performed by Transnetyx using verified protocols. Otherwise, no experimental procedures, drugs, or tests were performed on mice prior to the studies described.

Generation of Experimental Models

Ptn-GFP Mice: Sperm from *Ptn-EGFP* mice (Tg [Ptn-EGFP]), developed per the GENSAT Project at Rockefeller University, was obtained from the Mutant Mouse Resource and Research Center (MMRRC) and the strain was re-derived in a C57BL/6 background (Schmidt et al., 2013).

$Ptn^{fl/fl}$ mice: The Duke Cancer Institute BAC Recombineering Core designed targeting vectors for $Ptn^{fl/fl}$ mice (Liu et al., 2003). The Duke Transgenic Mouse Core injected the targeting vector into the G4 ES cell line (129S6/SvEvTac × C57BL/6Ncr). Positive ES clones were selected by Southern blotting and injected into C57BL/6J blastocysts, which were implanted in the uterus of female mice. Male chimeric mice were bred with C57BL/6J female mice and germline transmission was confirmed using PCR. Primers for genotyping $Ptn^{fl/fl}$ mice were ptn.S10: 5′-TCT TGC TTT CAC AAC TCC AGT GTC-3′ and ptn1.AS4 5′-TCC ACA GCT GCC AAG ATG AAA ATC-3′. Mice positive for the targeted allele were then backcrossed 6 generations into the C57BL/6 background before crossing into tissue specific Cre-recombinase mice in the C57BL/6 background. The following strains of tissue specific Cre-recombinase mice were purchased from Jackson laboratories (Bar Harbor, ME): *Osteocalcin-Cre, Leptin receptor-Cre, Vav1-Cre,* and *VE-cadherin-Cre.* Female $Ptn^{fl/fl}$ mice were backcrossed for two generations with Cre^{+} males to generate $Cre^{+};Ptn^{fl/fl}$ mice and $Cre;Ptn^{fl/fl}$ mice for experimental studies. For imaging studies, *ROSA26-TdTomato* (Jackson Laboratory) mice were crossed to various Cre lines to generate tissue specific reporters. All animal studies were performed using sex- and age-matched animals, with wild-type littermates as controls. Eight to12 week old adult mice were used for all studies.

METHOD DETAILS

Isolation of BMECs, $LepR^{+}$ cells and osteoblasts—BMECs were isolated using a modified version of the protocol published by Poulos et al. (Poulos et al., 2013). Intravital labeling of ECs was achieved via intravenous injection of 25 ug of anti-VEcadherin AF-647 (Biolegend, San Diego, CA) in 100 ul PBS into wild-type, 8 week old female C57BL/6 mice. Mice were euthanized 15 minutes following injection. Femurs and tibias were dissected, cleaned of adventitia, and crushed with a mortar and pestle. Crushed BM was digested for 10 minutes at 37°C in a 1 mg/ml solution of Liberase (Sigma-Aldrich, St. Louis, MO) in IMDM. Cells were rinsed in ice-cold PBS with 1% fetal bovine serum (FBS)(Fisher Scientific, Waltham, MA) and depleted of lineage-positive cells with the Miltenyi lineage depletion kit (Miltenyi Biotec Inc., San Diego, CA). The lineage negative fraction was stained with anti-CD45-V450 and 7AAD. Cells were sorted on a BD FACS ARIA (BD Biosciences) for the $7AAD^{-}CD45^{-}$ VE-$cadherin^{+}$ fraction. Cells from 5 female mice aged 8–10 weeks were pooled together to comprise one biological replicate. To isolate BM $LepR^{+}$ stromal cells, bones were crushed, digested, and lineage depleted as described above. The lineage negative fraction was stained with two antibodies for Leptin receptor: LepR-PE and LepR-FITC in addition to CD45 and 7AAD. Cells were sorted on a BD FACS ARIA for the $7AAD^{-}CD45^{-}$ $LepR^{+}$ subset.

BM osteolineage cells were isolated from *Osc-Cre;Ptn*$^{fl/fl}$ mice and littermate controls. Briefly, femurs and tibias were dissected and flushed with PBS to remove hematopoietic cells. Bones were then cleaned of adventitia and crushed with a mortar and pestle in PBS. Ground bone fragments of mouse femurs and tibias were digested × 3 hours with 0.2 mg/mL collagenase. Enzyme was inactivated with PBS^{+} 10% FBS, bone fragments were pelleted by centrifugation, and the digested bone chips were placed in 24 well plates (2–3 bone chips per well). Fragments were cultured for 3 days in DMEM-Ham F12 media containing 10% FBS, 0.1 mM L-ascorbic acid 2 phosphate, 2 mM L-glutamine, 100 U/ml penicillin and streptomycin. After 3 days, bone chips were removed and adherent colonies were observed; after 7 days, RNA was isolated from adherent cells for PTN expression analysis (Himburg et al., 2017).

Validation of cell-specific PTN deletion—In order to validate PTN deletion, PTN gene expression was assessed by qRT-PCR in isolated populations of BMECs, LepR^{+} cells, osteolineage cells and CD45^{+} hematopoietic cells from whole bone marrow. RNA from all cell populations was isolated using the QIAGEN RNeasy micro kit (QIAGEN, Hilden, Germany). RNA was reverse transcribed into cDNA using iScript cDNA synthesis kit. Real time PCR analysis for PTN and GAPDH was performed using Taqman Gene Expression assays (Life Technologies, Carlsbad, CA) on an Applied Biosystems QuantStudio 6 PCR Machine (Thermo Fisher Scientific, Canoga Park, CA). Data were normalized to GAPDH and littermate controls using the delta-CT method.

Flow cytometry—PB was collected from mice through sub-mandibular puncture. To collect BM cells, long bones (femurs and tibia) were harvested from euthanized mice and flushed with IMDM containing 10% FBS. BM cells were filtered through a 40 mm strainer to obtain single cell suspension. Both PB samples and BM cells were lysed with RBC lysis buffer priorto FACs staining. BM cells from non-irradiated and irradiated mice were analyzed by FACS analysis for myeloid (Mac-1^{+}Gr-1^{+}), lymphoid (B220^{+}), progenitor (lineage negative, ckit^{+}, sca1^{-}, and HSC subsets (lineage negative, ckit^{+}, sca1^{+}, CD150^{+}, CD41^{-}, CD48^{-}). Samples were stained at 4°C in the dark for 30 minutes, rinsed with PBS containing 10% FBS, and resuspended in 400 ul of bufferfor FACS analysis. To discriminate dead cells, 7AAD was added to each sample immediately prior to analysis. Analysis was performed on a BD Canto II FACS instrument.

Colony forming cell assay—CFC assays [colony forming unit-granulocyte monocyte (CFU-GM), burst forming unit-erythroid (BFU-E), and colony forming unit-granulocyte erythroid monocyte megakaryocyte (CFU-GEMM)] were performed as follows based on established protocols (Yan et al., 2016). BM cells were depleted of red blood cells using ACK (Ammonium-Chloride-Potassium) red cell lysis buffer, resuspended in IMDM +10% FBS +1% P/S, and filtered through a 30 um cell strainer. Cells were enumerated using a BioRad TC10 Automated Cell counter (BioRad Laboratories, Hercules, CA). Ten thousand live BM cells were resuspended per 1 mL of methylcellulose M3434 medium (StemCell Technologies, Vancouver, Canada) and plated in one 35 mm gridded CFC dish (StemCell Technologies). After 14 days, colonies were enumerated.

Competitive Repopulation Assays—For primary competitive repopulation assays, BM cells from donor 10–12 week old female mice were isolated. Recipient 10 week old female CD45.1$^+$ B6.SJL mice were irradiated with 900 cGy TBI using a Cs137 irradiator and transplanted with 2×10^5 donor BM cells via tail vein injection along with a competing dose of 2×10^5 competitor CD45.1$^+$ BM cells. For secondary competitive repopulation assays, 1×10^6 BM cells from primary recipient mice were transplanted along with 2×10^5 competitor CD45.1$^+$ BM cells. Multilineage donor hematopoietic cell engraftment was measured in the PB by flow cytometry using an established protocol (Himburg et al., 2017; Yan et al., 2016). Peripheral blood was red blood cell depleted with ACK lysis buffer, rinsed with PBS containing 10% FBS, and resuspended in a volume of 400 ul. Each sample was stained for CD45.2 FITC, CD45.1 PE, B220 APC-CY7, Gr-1 PE, Mac-1 PE, CD3 V450, and Ter119 APC. Samples were stained at 4°C in the dark for 30 minutes and rinsed with PBS containing 10% FBS, and resuspended in 400 ul of buffer for FACS analysis.

For primary competitive repopulation assays from irradiated donor mice (CD45.2$^+$), BM cells were collected from donor mice at day 10 following 500 cGy TBI. Recipient CD45.1$^+$ mice were irradiated with 900 cGy TBI and then transplanted with 1×10^6 donor BM cells, along with 2×10^5 competitor CD45.1$^+$ BM cells. Secondary competitive repopulation assays were performed using 3×10^6 BM cells from primary recipient mice, along with a competing dose of 2×10^5 non-irradiated host BM cells.

Microscopic imaging and immunofluorescence analysis—Animals were tail vein injected with 25 μg of VE-Cadherin Alexa-647 antibody (Biolegend) 20 minutes prior to euthanasia. Femurs were extracted and muscle and connective tissue was cleaned. The bones were fixed in 4% paraformaldehyde for 4 hours at 4°C. Bones were washed 3 times with PBS at 4°C and then moved to decalcify in ice cold 0.5M EDTA pH = 7.4 overnight at 4°C, shaking. The following day, the femurs were washed 3 times with PBS and moved to 10 mL of ice-cold cryoprotectant solution (20% sucrose/20% PVP weight/volume) and incubated at 4°C overnight. The next day, the bones were moved to 10mL warm embedding (EBM) solution (8g gelatin, 2g PVP, 20 g sucrose in 100ml PBS). The samples in EBM were then incubated in a water bath set to 60°C for 45 minutes. Following incubation, samples were moved to tissue molds that are filled with EBM. Samples were incubated for 30 minutes at room temperature and then blocks were transferred to a −80°C freezer. The following day, sections were made using a Leica Cryostat cooled to −23°C. 100 micron sections were made and transferred to Superfrost Plus microscope slides. The slides were labeled by rehydrating the sample with 200 ml PBS and then permeabilizing with 0.5% triton/PBS for 20 minutes at room temperature. Slides were blocked with 5% FBS/permeabilization buffer for 30 minutes at room temperature. Slides were labeled using an anti-GFP antibody (Aves, GFP-1020, 1:200) for 1 hour at room temperature. The slide was then washed 3 times and incubated with an anti-chicken-DyLight-488 secondary antibody. The slide was then washed 3 times and incubated with DAPI (Biolegend, 1:1000) for 20 minutes. A slide labeled with secondary antibody only was used to set the microscope gain for imaging. The slide was then washed and mounted using Fluoromount (Sigma-Aldrich). Slides were sealed and allowed to dry overnight before imaging. Imaging was performed on a Leica SP8 confocal microscope using a 40× oil objective. Bidirectional scanning was enabled and imaging was

performed sequentially using a UV or white light laser set to 488nm, 561nm or 647nm for excitation. Fluorescence emission was detected on a PMT or HyD SMD detector. Images were deconvoluted using Huygens Professional software (Scientific Volume Imaging, the Netherlands). Images were rendered in *ImageJ* and the same settings were applied to images. Co-localization quantification of 290.91 × 290.91 micron field of view was performed using the Just Another Colocalization Plugin (JACoP) in *ImageJ* to calculate the Mander's coefficient. Confocal laser scanning microscopy was performed at the California Nanosystems Institute Advanced Light Microscopy Shared Resource Facility at UCLA.

Vessel Morphology—Slides were prepared as described above. Sections were labeled with CD31-Alexa-647 (Biolegend #102516) and imaged using a Leica SP8 confocal microscope equipped with a 40× oil objective. Maximum intensity projections were generated in the Leica LAS X software and exported as TIFF files for analysis using *AngioTool* software (Zudaire et al., 2011). *AngioTool* settings used were diameter = 12, intensity 20–255, remove small particles = 24 and fill holes = 120.

Adipocyte Quantification—Thresholds for images were set and converted to 8-bit binary images in *Fiji* software. The holes were filled in the binary images and watershed separation was applied. The 'analyze particles' function was used to quantify the number of adipocytes per field of view (particle size = 5500–12000 px; circularity = 0.05–1, particles on edges excluded). Fields of view analyzed were 624.7×501.22 microns.

ELISA—Whole BM from one mouse femur was flushed into 400 ul of PBS in a 1.5 mL Eppendorf tube. After centrifugation, 1X BM supernatants were collected and analyzed for PTN protein levels using a mouse PTN ELISA kit (Lifespan Biosciences, Seattle, WA).

Radiation Studies—8 week old female *VECad-Cre;Ptn$^{fl/fl}$* mice, *LepR-Cre;Ptn$^{fl/fl}$* mice, and *Cre*$^{-}$ littermate control mice were irradiated with 500 cGy or 700 cGy TBI using a Cesium-137 irradiator. For all studies, both male and female littermates were used. Equal numbers of male and female mice from each genotype were used. PB and BM cells were collected from mice in each group at day +10 for analysis of hematopoiesis. Complete blood counts were measured using a Hemavet 950 instrument (Drew Scientific, Oxford, CT). For survival studies, mice were monitored daily through day +60 and euthanized as proscribed by our animal use protocol, if necessary.

QUANTIFICATION AND STATISTICAL ANALYSIS

Values are represented as means ± SEM, unless stated otherwise. GraphPad Prism 6.0 was utilized for all statistical analyses. All data were checked for normal distribution and similar variance between groups. The choice of statistical test was based on the numbers of groups and variables. In the case of one-way and two-way ANOVA analyses, reported p values are based on multiple test corrections. Data in all functional studies were derived from 3 or more independent experiments from distinct mice or cell culture plates. Sample size for *in vitro* studies was chosen based on observed effect sizes and standard errors from prior studies. For animal studies, a powertest was used to determine the sample size needed to observe a 2-fold difference in mean between groups with 0.8 power using a 2-tailed Student's t test. All

animal studies were performed using sex- and age-matched animals, with wild-type littermates as controls. Animal studies were performed without blinding of the investigator and no animals were excluded from the analysis. Statistical details of each experiment can be found in the Figure Legends, including the numbers of replicates and p values from comparative analyses that were performed.

Supplementary Material

Refer to Web version on PubMed Central for supplementary material.

ACKNOWLEDGMENTS

This work was supported by NHLBI grant HL-086998 (to J.P.C.), NIAID grants AI-067769 and AI-107333 (to J.P.C.), California Institute for Regenerative Medicine leadership award LA1-08014 (to J.P.C.), NIAID grant AI-138331 (to H.A.H.), and the Damon Runyon fellowship award DRG-2327-18 (to C.M.T.).

REFERENCES

Acar M, Kocherlakota KS, Murphy MM, Peyer JG, Oguro H, Inra CN, Jaiyeola C, Zhao Z, Luby-Phelps K, and Morrison SJ (2015). Deep imaging of bone marrow shows non-dividing stem cells are mainly perisinusoidal. Nature 526, 126–130. [PubMed: 26416744]

Alva JA, Zovein AC, Monvoisin A, Murphy T, Salazar A, Harvey NL, Carmeliet P, and Iruela-Arispe ML (2006). VE-Cadherin-Cre-recombinase transgenic mouse: a tool for lineage analysis and gene deletion in endothelial cells. Dev. Dyn 235, 759–767. [PubMed: 16450386]

Asada N, Kunisaki Y, Pierce H, Wang Z, Fernandez NF, Birbrair A, Ma'ayan A, and Frenette PS (2017). Differential cytokine contributions of perivascular haematopoietic stem cell niches. Nat. Cell Biol 19, 214–223. [PubMed: 28218906]

Cashman JD, and Eaves CJ (1999). Human growth factor-enhanced regeneration of transplantable human hematopoietic stem cells in nonobese diabetic/severe combined immunodeficient mice. Blood 93, 481–487. [PubMed: 9885209]

Chauhan AK, Li YS, and Deuel TF (1993). Pleiotrophin transforms NIH 3T3 cells and induces tumors in nude mice. Proc. Natl. Acad. Sci. USA 90, 679–682. [PubMed: 8421705]

Chen JY, Miyanishi M, Wang SK, Yamazaki S, Sinha R, Kao KS, Seita J, Sahoo D, Nakauchi H, and Weissman IL (2016). Hoxb5 marks long-term haematopoietic stem cells and reveals a homogenous perivascular niche. Nature 530, 223–227. [PubMed: 26863982]

Christman KL, Fang Q, Yee MS, Johnson KR, Sievers RE, and Lee RJ (2005). Enhanced neovasculature formation in ischemic myocardium following delivery of pleiotrophin plasmid in a biopolymer. Biomaterials 26, 1139–1144. [PubMed: 15451633]

Ding L, and Morrison SJ (2013). Haematopoietic stem cells and early lymphoid progenitors occupy distinct bone marrow niches. Nature 495, 231–235. [PubMed: 23434755]

Ding L, Saunders TL, Enikolopov G, and Morrison SJ (2012). Endothelial and perivascular cells maintain haematopoietic stem cells. Nature 481, 457–462. [PubMed: 22281595]

Doan PL, Himburg HA, Helms K, Russell JL, Fixsen E, Quarmyne M, Harris JR, Deoliviera D, Sullivan JM, Chao NJ, et al. (2013). Epidermal growth factor regulates hematopoietic regeneration after radiation injury. Nat. Med 19, 295–304. [PubMed: 23377280]

Dominici M, Rasini V, Bussolari R, Chen X, Hofmann TJ, Spano C, Bernabei D, Veronesi E, Bertoni F, Paolucci P, et al. (2009). Restoration and reversible expansion of the osteoblastic hematopoietic stem cell niche after marrow radioablation. Blood 114, 2333–2343. [PubMed: 19433859]

Goncalves KA, Silberstein L, Li S, Severe N, Hu MG, Yang H, Scadden DT, and Hu GF (2016). Angiogenin promotes hematopoietic regeneration by dichotomously regulating quiescence of stem and progenitor cells. Cell 166, 894–906. [PubMed: 27518564]

Greenbaum A, Hsu YM, Day RB, Schuettpelz LG, Christopher MJ, Borgerding JN, Nagasawa T, and Link DC (2013). CXCL12 in early mesenchymal progenitors is required for haematopoietic stem-cell maintenance. Nature 495, 227–230. [PubMed: 23434756]

Guo P, Poulos MG, Palikuqi B, Badwe CR, Lis R, Kunar B, Ding BS, Rabbany SY, Shido K, Butler JM, and Rafii S (2017). Endothelial jagged-2 sustains hematopoietic stem and progenitor reconstitution after myelosuppression. J. Clin. Invest 127, 4242–4256. [PubMed: 29058691]

Gupta P, Oegema TR Jr., Brazil JJ, Dudek AZ, Slungaard A, and Verfaillie CM (2000). Human LTC-IC can be maintained for at least 5 weeks in vitro when interleukin-3 and a single chemokine are combined with O-sulfated heparan sulfates: requirement for optimal binding interactions of heparan sulfate with early-acting cytokines and matrix proteins. Blood 95, 147–155. [PubMed: 10607697]

Himburg HA, Muramoto GG, Daher P, Meadows SK, Russell JL, Doan P, Chi JT, Salter AB, Lento WE, Reya T, et al. (2010). Pleiotrophin regulates the expansion and regeneration of hematopoietic stem cells. Nat. Med 16, 475–482. [PubMed: 20305662]

Himburg HA, Harris JR, Ito T, Daher P, Russell JL, Quarmyne M, Doan PL, Helms K, Nakamura M, Fixsen E, et al. (2012). Pleiotrophin regulates the retention and self-renewal of hematopoietic stem cells in the bone marrow vascular niche. Cell Rep. 2, 964–975. [PubMed: 23084748]

Himburg HA, Yan X, Doan PL, Quarmyne M, Micewicz E, McBride W, Chao NJ, Slamon DJ, and Chute JP (2014). Pleiotrophin mediates hematopoietic regeneration via activation of RAS. J. Clin. Invest 124, 4753–4758. [PubMed: 25250571]

Himburg H, Doan P, Quarmyne M, Yan X, Sasine J, Zhao L, Hancock GV, Kan J, Pohl KA, Tran E, et al. (2017). Dickkopf-1 promotes hematopoietic regeneration via direct and niche-mediated mechanisms. Nat. Med 23, 91–99. [PubMed: 27918563]

Hooper A, Butler J, Nolan D, Kranz A, Iida K, Kobayashi M, Kopp HG, Shido K, Petit I, Yanger K, et al. (2009). Engraftment and reconstitution of hematopoiesis is dependent on VEGFR2-mediated regeneration of sinusoidal endothelial cells. Cell Stem Cell 4, 263–274. [PubMed: 19265665]

Itkin T, Gur-Cohen S, Spencer JA, Schajnovitz A, Ramasamy SK, Kusumbe AP, Ledergor G, Jung Y, Milo I, Poulos MG, et al. (2016). Distinct bone marrow blood vessels differentially regulate hematopoiesis. Nature 532, 323–328. [PubMed: 27074509]

Kinnunen T, Raulo E, Nolo R, Maccarana M, Lindahl U, and Rauvala H (1996). Neurite outgrowth in brain neurons induced by heparin-binding growth associated molecule (HB-GAM) depends on the specific interaction of HB-GAM with heparan sulfate at the cell surface. J. Biol. Chem 271, 2243–2248. [PubMed: 8567685]

Kusumbe AP, Ramasamy SK, Itkin T, Mäe MA, Langen UH, Betsholtz C, Lapidot T, and Adams RH (2016). Age-dependent modulation of vascular niches for haematopoietic stem cells. Nature 532, 380–384. [PubMed: 27074508]

Laaroubi K, Delbe J, Vacherot F, Desgranges P, Tardieu M, Jaye M, Barritault D, and Courty J (1994). Mitogenic and in vitro angiogenic activity of human recombinant heparin affin regulatory peptide. Growth Factors 10, 89–98. [PubMed: 7520717]

Liu P, Jenkins NA, and Copeland NG (2003). A highly efficient recombineering-based method for generating conditional knockout mutations. Genome Res. 13, 476–484. [PubMed: 12618378]

Lucas D, Scheiermann C, Chow A, Kunisaki Y, Bruns I, Barrick C, Tessarollo L, and Frenette PS (2013). Chemotherapy-induced bone marrow nerve injury impairs hematopoietic regeneration. Nat. Med 19, 695–703. [PubMed: 23644514]

Michelotti GA, Tucker A, Swiderska-Syn M, Machado MV, Choi SS, Kruger L, Soderblom E, Thompson JW, Mayer-Salman M, Himburg HA, et al. (2016). Pleiotrophin regulates the ductular reaction by controlling the migration of cells in liver progenitor niches. Gut 65, 683–692. [PubMed: 25596181]

Na Nakorn T, Traver D, Weissman IL, and Akashi K (2002). Myeloerythroid-restricted progenitors are sufficient to confer radioprotection and provide the majority of day 8 CFU-S. J. Clin. Invest 109, 1579–1585. [PubMed: 12070305]

Netelenbos T, van den Born J, Kessler FL, Zweegman S, Merle PA, van Oostveen JW, Zwaginga JJ, Huijgens PC, and Dräger AM (2003). Proteoglycans on bone marrow endothelial cells bind and

present SDF-1 towards hematopoietic progenitor cells. Leukemia 17, 175–184. [PubMed: 12529676]

Osawa M, Hanada K, Hamada H, and Nakauchi H (1996). Long-term lymphohematopoietic reconstitution by a single CD34-low/negative hematopoietic stem cell. Science 273, 242–245. [PubMed: 8662508]

Perez-Pinera P, Berenson JR, and Deuel TF (2008). Pleiotrophin, a multifunctional angiogenic factor: mechanisms and pathways in normal and pathological angiogenesis. Curr. Opin. Hematol 15, 210–214. [PubMed: 18391787]

Poulos MG, Guo P, Kotier NM, Pinho S, Gutkin MC, Tikhonova A, Aifantis I, Frenette PS, Kitajewski J, Rafii S, and Butler JM (2013). Endothelial Jagged-1 is necessary for homeostatic and regenerative hematopoiesis. Cell Rep. 4, 1022–1034. [PubMed: 24012753]

Raaijmakers MH, Mukherjee S, Guo S, Zhang S, Kobayashi T, Schoonmaker JA, Ebert BL, Al-Shahrour F, Hasserjian RP, Scadden EO, et al. (2010). Bone progenitor dysfunction induces myelodysplasia and secondary leukaemia. Nature 464, 852–857. [PubMed: 20305640]

Ruiz-Herguido C, Guiu J, D'Altri T, Ingles-Esteve J, Dzierzak E, Espinosa L, and Bigas A (2012). Hematopoietic stem cell development requires transient Wnt/β-catenin activity. J. Exp. Med 209, 1457–1468. [PubMed: 22802352]

Salter AB, Meadows SK, Muramoto GG, Himburg H, Doan P, Daher P, Russell L, Chen B, Chao NJ, and Chute JP (2009). Endothelial progenitor cell infusion induces hematopoietic stem cell reconstitution in vivo. Blood 113,2104–2107. [PubMed: 19141867]

Schmidt EF, Kus L, Gong S, and Heintz N (2013). BAC transgenic mice and the GENSAT database of engineered mouse strains. Cold Spring Harb. Protoc 2013, 200–206.

Yan X, Himburg HA, Pohl K, Quarmyne M, Tran E, Zhang Y, Fang T, Kan J, Chao NJ, Zhao L, et al. (2016). Deletion of the Imprinted Gene Grb10 Promotes Hematopoietic Stem Cell Self-Renewal and Regeneration. Cell Rep. 17, 1584–1594. [PubMed: 27806297]

Yang L, Bryder D, Adolfsson J, Nygren J, Mansson R, Sigvardsson M, and Jacobsen SE (2005). Identification of Lin(−)Sca1(+)kit(+)CD34(+)Flt3-short-term hematopoietic stem cells capable of rapidly reconstituting and rescuing myeloablated transplant recipients. Blood 105, 2717–2723. [PubMed: 15572596]

Zandstra PW, Conneally E, Petzer AL, Piret JM, and Eaves CJ (1997). Cytokine manipulation of primitive human hematopoietic cell self-renewal. Proc Natl Acad Sci USA. 94, 4698–703. [PubMed: 9114054]

Zhou BO, Ding L, and Morrison SJ (2015). Hematopoietic stem and progenitor cells regulate the regeneration of their niche by secreting Angiopoietin-1. eLife 4, e05521. [PubMed: 25821987]

Zhou BO, Yu H, Yue R, Zhao Z, Rios JJ, Naveiras O, and Morrison SJ (2017). Bone marrow adipocytes promote the regeneration of stem cells and haematopoiesis by secreting SCF. Nat. Cell Biol 19, 891–903. [PubMed: 28714970]

Zudaire E, Gambardella L, Kurcz C, and Vermeren S (2011). A computational tool for quantitative analysis of vascular networks. PLoS One 6, e27385. [PubMed: 22110636]

Highlights

- PTN secretion by BM stromal cells is essential for HSC maintenance
- Hematologic recovery following irradiation requires PTN from BM stromal cells and ECs
- PTN secretion by BMECs is essential for HSC regeneration following irradiation
- Irradiation enriches for PTN-expressing BMECs in the niche

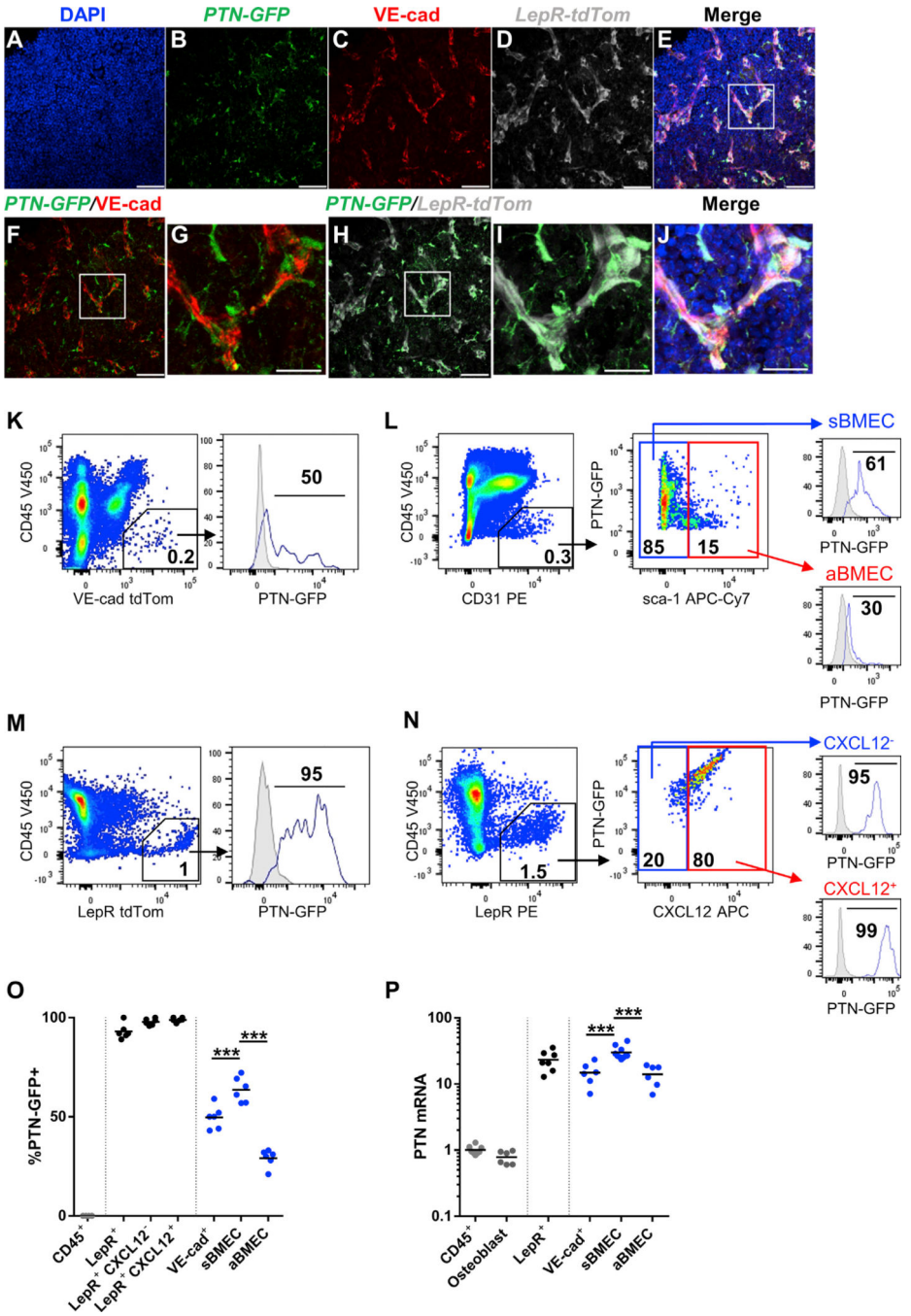

Figure 1. PTN Is Expressed by VE-cad$^+$ ECs and LepR$^+$ Stromal Cells in the BM Vascular Niche

(A–J) Representative 40× confocal images of 100-μm femur sections from *LepRCre;ROSA26-TdTomato;PTN – EGFP* mice showing DAPI nuclear counterstain (A, blue), PTN expression (B, green), VE-cad expression (C, red), and LepR expression (D, white). Merged image is shown in (E). Scale bars, 50 μm. Co-localization of PTN and VE-cad expression is shown at 40× (F) and magnified in (G). Co-localization of PTN and LepR expression is shown at 40× in (H) and magnified in (I). (J) Shows merged image of PTN, VE-cad, and LepR expression in the BM. Scale bar, 20 μm (G, I, and J).

(K) Left: representative flow cytometric analysis of BM $CD45^{-}VE\text{-}cad^{+}$ ECs at baseline. Right: histogram showing PTN expression by$CD45^{-}VE\text{-}cad^{+}$ ECs. Isotype control is shown in gray. Numbers represent the percentages of cells within the gate.

(L) Left: representative flow cytometric analysis of BM $CD45^{-}CD31^{+}$ ECs. Right: representative analysis of $CD31^{+}Sca\text{-}1^{-}$ sinusoidal BMECs (sBMECs) and $CD31^{+}Sca\text{-}1^{+}$ arteriolar BMECs (aBMECs) at baseline.

(M) Representative flow cytometric analysis of BM $CD45^{-}LepR^{+}$ stromal cells and PTN expression in $CD45^{-}LepR^{+}$ cells.

(N) Representative analysis of CXCL12 expression by BM $CD45^{-}LepR^{+}$ stromal cells and PTN expression by BM $LepR^{+}CXCL12^{+}$ and $LepR^{+}CXCL12^{-}$ cells.

(O) Mean percentages of $PTN\text{-}GFP^{+}$ cells within the BM populations shown. ***$p < 0.001$, $n = 6$/group.

(P) Scatterplots of mean PTN mRNA levels in the BM populations shown. ***$p < 0.001$, $n = 6–8$/group.

Expression levels were normalized to CD45 and glyceraldehyde-3 phosphate dehydrogenase (GAPDH) expression; one-way ANOVA with Dunnett’s multiple comparison test. See also Figure S1.

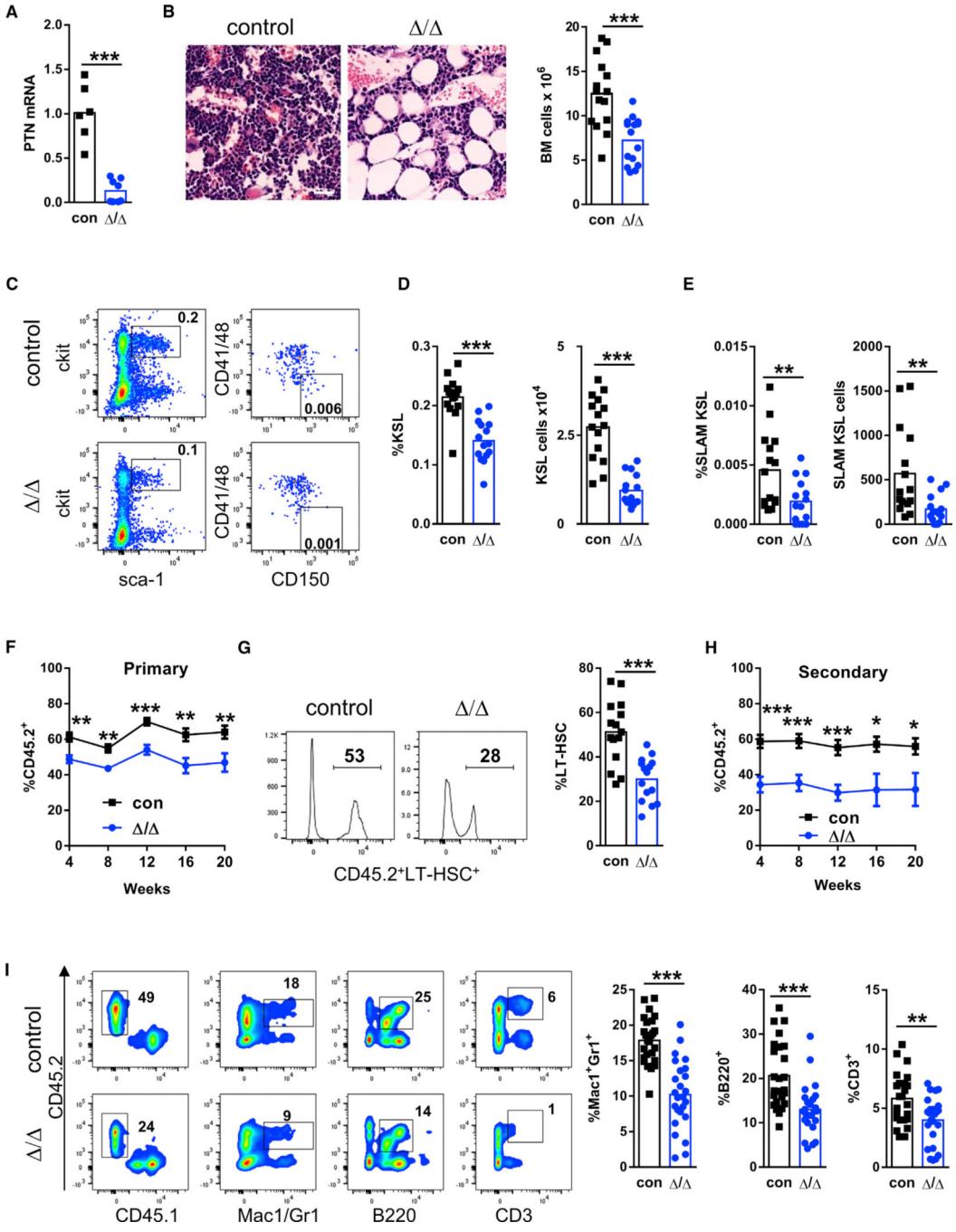

Figure 2. HSC Maintenance Requires PTN from LepR$^+$ Stromal Cells

(A) Mean levels of *Ptn* mRNA In BM LepR$^+$ cells from *LepR-Cre;Ptn $^{fl/fl}$* mice (Δ/Δ) relative to LepR$^+$ cells from *Cre$^-$;Ptn $^{fl/fl}$* mice (control [con]). ***p < 0.001, n = 6–8/group. (B) Left: representative microscopic images (40×) of BM cellularity in *LepR-Cre;Ptn $^{fl/fl}$* mice (Δ/Δ) and *Cre$^-$;Ptn $^{fl/fl}$* mice (control) are shown. Scale bar, 50 μm. Right: mean BM cell counts per femur for each group. ***p < 0.001, n = 15/group.

(C) Representative flow cytometric analysis of BM KSL cells and CD41/48^{-}CD150^{+} KSL (SLAM KSL) cells in *LepR-Cre;PTN* $^{fl/fl}$ mice versus control mice. Numbers represent the percentage of cells within the gates.

(D) Mean percentage of KSL cells and KSL cells per femur are shown for each group. ***p < 0.001, n = 15/group.

(E) Mean percentage of SLAM KSL cells and numbers of SLAM KSL cells are shown for *LepR-Cre;Ptn* $^{fl/fl}$ mice and control mice. **p < 0.01, n = 15/group.

(F) Mean donor CD45.2^{+} cell engraftment overtime in the PB of recipient CD45.1^{+} mice following transplantation of 2 × 10^{5} BM cells from *Lep-RCre;Ptn*$^{fl/fl}$ mice or control mice and 2 × 10^{5} competitor CD45.1^{+} BM cells. **p < 0.01, ***p < 0.001, n = 10–25/group. A two-way ANOVA with Sidak's multiple comparisons test was performed. Data represent means ± SEM.

(G) Left: representative donor percentage of CD45.2^{+} CD34^{-}Flt-3^{-}KSL cells (LT-HSCs) are shown at 12 weeks in the BM of recipient mice transplanted with BM cells from control mice and *LepR-Cre;Ptn* $^{fl/fl}$ mice (Δ/Δ). Right: mean percentages of CD45.2^{+} LT-HSCs are shown for each group. ***p < 0.001, n = 15/group.

(H) Mean donor CD45.2^{+} cell engraftment overtime in the PB of secondary recipient CD45.1^{+} mice transplanted with 1 × 10^{6} BM cells from primary recipient mice along with 2 × 10^{5} competitor CD45.1^{+} BM cells. *p < 0.05, ***p < 0.001, n = 10–25/group. A two-way ANOVA with Sidak's multiple comparisons test was performed. Data represent means ± SEM.

(I) Left: representative flow cytometric analysis of multilineage donor CD45.2^{+} cell engraftment at 12 weeks in the BM of secondary transplanted CD45.1^{+} mice in the groups shown. Right: mean values for donor CD45.2^{+} myeloid cells (Mac1^{+}Gr1^{+}), B cells (B220^{+}), and T cells (CD3^{+}) in secondary transplanted mice from the two groups are shown. **p < 0.01, ***p < 0.001, n = 25/group.

We performed two-sided Student's t test for all analyses other than indicated. See also Figures S2 and S3.

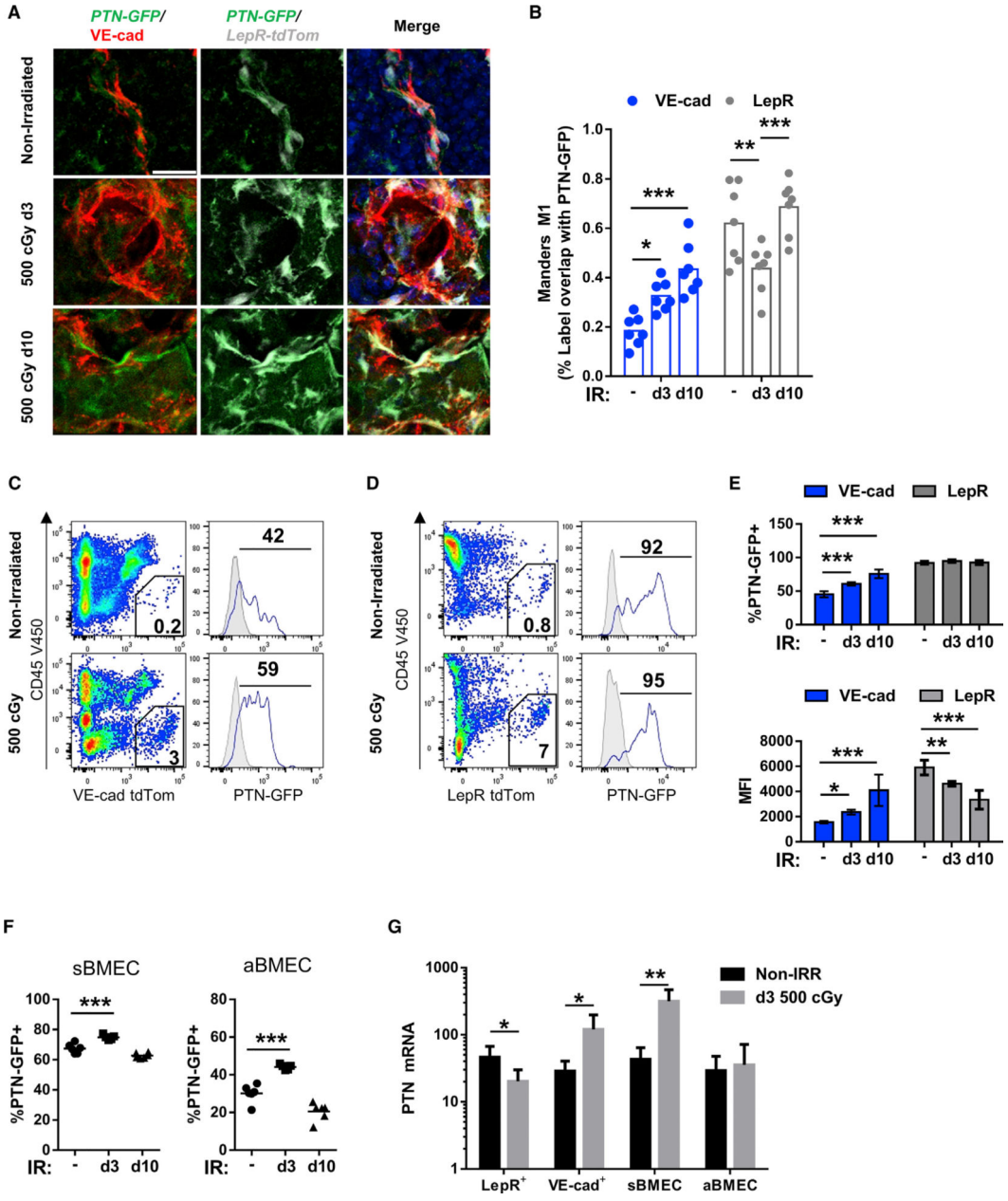

Figure 3. Irradiation Enriches for PTN-Expressing BMECs

(A) Representative magnified confocal images (40×) from 100-μm femur sections isolated from *LepRCre;ROSA26-TdTomato;Ptn – EGFP* mice and stained with DAPI, anti-GFP, and VE-cad Alexa 647. Maximum z-intensity projections are shown from non-irradiated mice and 3 days and 10 days following 500 cGy TBI. Scale bar, 20 μm.

(B) Manders correlation analysis was performed using the JACOP plug-in in ImageJ. Each data point represents the average Mander's coefficient (M1)from one field of view from n = 3 independent experiments and n = 7 fields of view analyzed. *p < 0.05, **p < 0.01, ***p < 0.001; *post hoc* unpaired t test with Bonferroni correction following one-way ANOVA analysis.

(C) Representative flow cytometric analysis of BM $CD45^{-}VE\text{-}cad^{+}$ ECs and PTN expression within $CD45^{-}VE\text{-}cad^{+}$ ECs in non-irradiated mice and on day +3 following 500 cGy TBI.

(D) Representative flow cytometric analysis of BM $CD45^{-}LepR^{+}$ stromal cells and PTN expression within $CD45^{-}LepR^{+}$ stromal cells in non-irradiated mice and on day +3 following 500 cGy TBI.

(E) Top: mean percentages of $PTN^{+}VE\text{-}cad^{+}$ ECs and $PTN^{+}LepR^{+}$ stromal cells in non-irradiated mice and over time following 500 cGy TBI. Bottom: the mean fluorescence intensity (MFI) of PTN expression in $VE\text{-}cad^{+}$ ECs and $LepR^{+}$ stromal cells is shown in non-irradiated mice and over time following 500 cGy TBI. *$p < 0.05$, **$p < 0.01$, ***$p < 0.001$, n = 6/group, two-way ANOVA. Data represent means ± SD.

(F) Scatterplots showing the percentages of $PTN^{+}CD31^{+}Sca\text{-}1^{-}$ sBMECs and $PTN^{+}CD31^{+}Sca\text{-}1^{+}$ aBMECs in non-irradiated mice and over time following 500 cGy TBI. ***$p < 0.001$, n = 6/group, one-way ANOVA.

(G) Bar graph showing the fold change in PTN gene expression within the BM cell populations shown. mRNA levels were normalized to CD45 and GAPDH expression. *$p < 0.05$, n = 4–9/group, multiple t test with Holm-Sidak correction. Mean values ± SD are shown.

See also Figure S4.

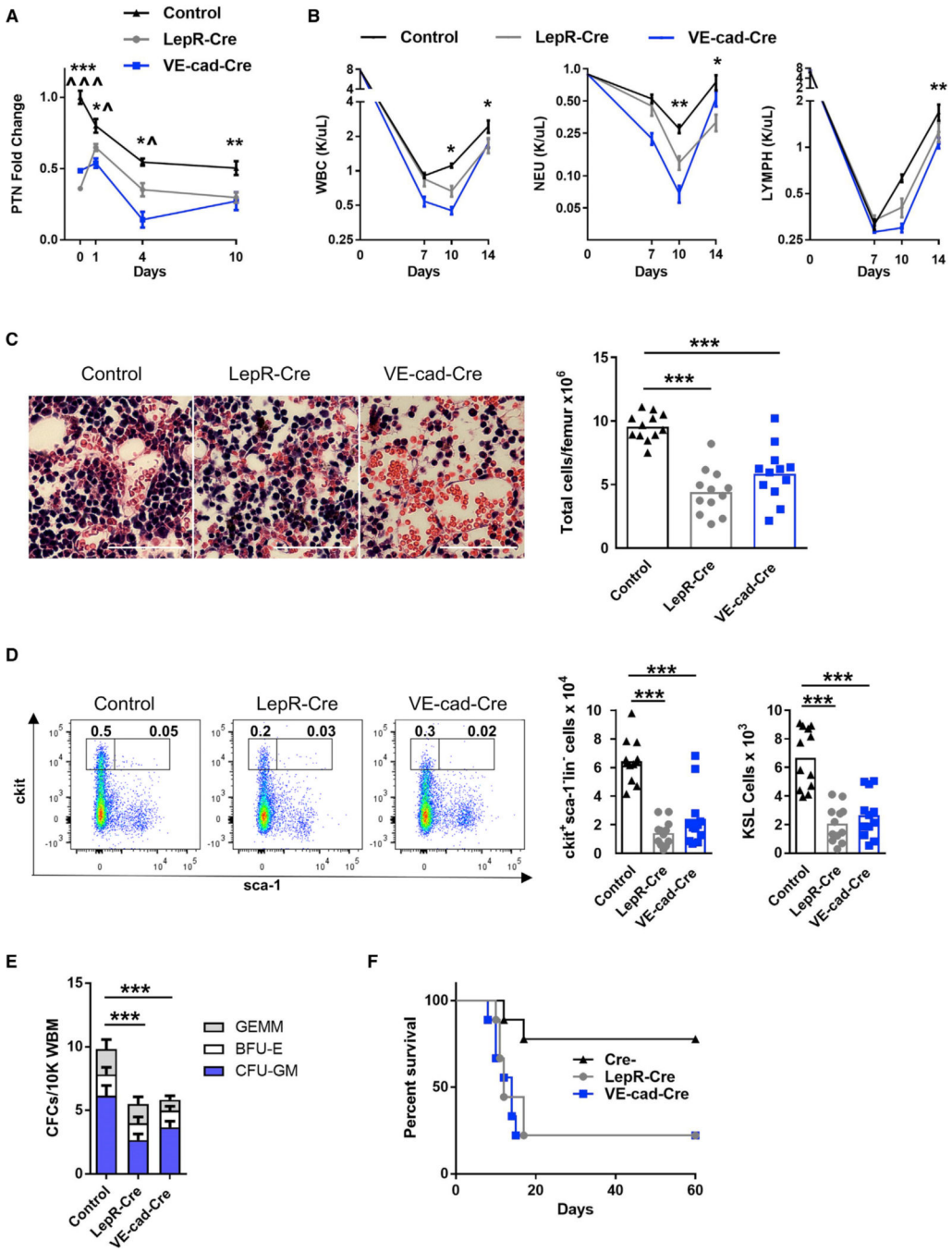

Figure 4. PTN Is Required from LepR$^+$ Stromal Cells and VEcad$^+$ ECs for Hematologic Recovery and Survival after Irradiation

(A) Mean levels of PTN In the BM of control mice (Cre$^-$), *LepR-Cre;Ptn* $^{fl/fl}$ mice (LepR-Cre) and *VE-cadCre;Ptn* $^{fl/fl}$ mice (VE-cad-Cre) at steady state (non-Irradlated) and on day +1, day +4, and day +10 after 500 cGy TBI. *$p < 0.05$, **$p < 0.01$, and ***$p < 0.001$ for comparison of controls with both LepR-Cre and VE-cad-Cre mice. ^$p < 0.05$ and ^^^$p < 0.001$ for comparison of LepR-Cre with VE-cad-Cre mice. n = 4–10/group; two-way ANOVA with Tukey multiple comparisons test. Data represent means ± SEM.

(B) PB white blood cell (WBC), neutrophil (NEU), and lymphocyte (LYMPH) counts in non-irradiated mice, LepR-Cre mice, and VE-cad-Cre mice and overtime following 500 cGy TBI. *$p < 0.05$ and **$p < 0.01$ for comparison of control mice with LepR-Cre and VE-cad-Cre mice. n = 5–12/group; two-way ANOVA with Dunnett's multiple comparisons test. Data represent means ± SEM.

(C) Left: representative H&E images (20×) from the mouse groups shown on day +10 following 500 cGy TBI. Scale bars, 100 μm. Right: mean BM cell counts from each group. ***$p < 0.001$, n = 12/group; one-way ANOVA with Dunnett's multiple comparisons test.

(D) Left: representative flow cytometric analysis of percentages of BM ckit^{+}sca-1^{-}lin^{-} cells and KSL cells in the mouse groups shown on day +10. Right, mean numbers of BM ckit^{+}sca-1^{-}lin^{-} myeloid progenitor cells and KSL cells in each group on day +10. ***$p < 0.001$; n = 12/group; one-way ANOVA with Dunnett's multiple comparisons test.

(E) Mean numbers of BM CFCs in the groups shown on day +10 following 500 cGy TBI. ***$p < 0.01$, n = 6/group; two-way ANOVA with Dunnett's multiple comparisons test. Data represent means ± SEM.

(F) Percent survival of the mice groups shown through day +60 following 700 cGy TBI. p = 0.01 for controls versus *LepR-Cre;Ptn* $^{fl/fl}$ mice, p = 0.01 for controls versus *VE-cad-Cre;Ptn* $^{fl/fl}$ mice, n = 9/group, log rank test for survival analysis.

See also Figure S4.

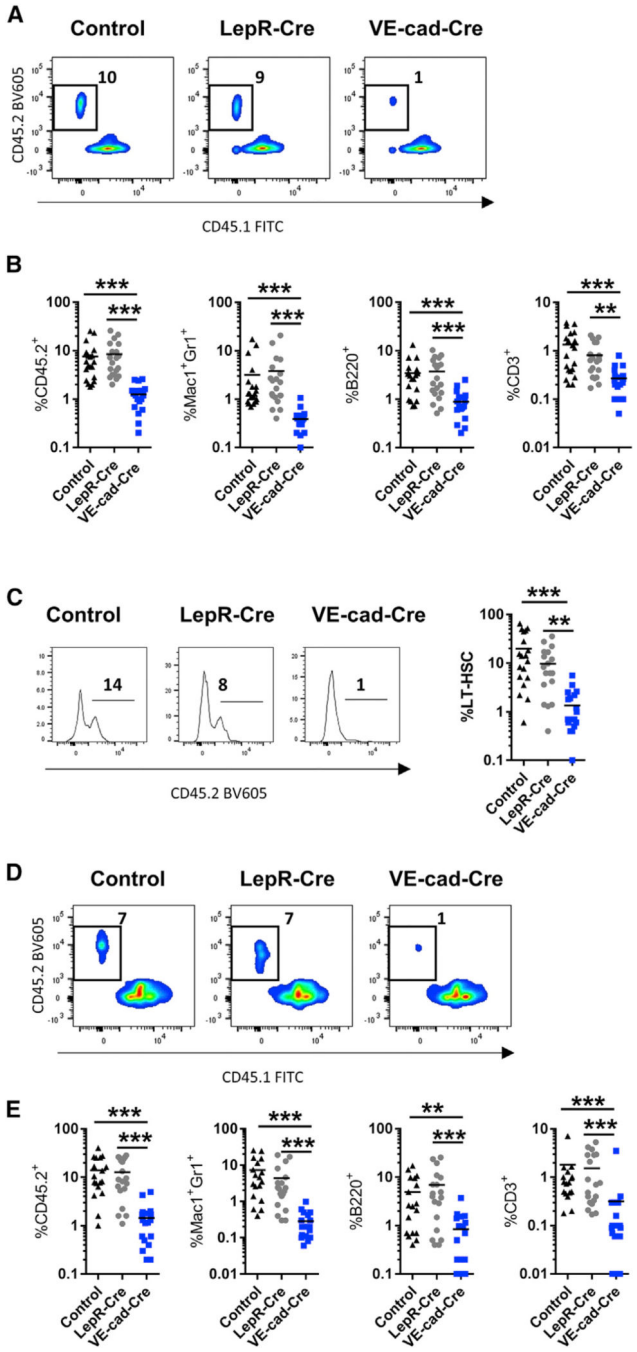

Figure 5. HSC Regeneration Requires PTN from VE-cad$^+$ ECs

(A) Representative flow cytometric plots show decreased engraftment of donor CD45.2$^+$ cells in the BM of CD45.1$^+$ recipient mice 12 weeks following transplantation of 1 × 10^6 BM CD45.2$^+$ cells collected from irradiated control mice, *LepR-Cre;Ptn* $^{fl/fl}$ mice, or *VE-cad-Cre;Ptn* $^{fl/fl}$ mice along with 2 × 10^5 competitor CD45.1$^+$ BM cells.

(B) Scatterplots showing mean total donor CD45.2$^+$ cell engraftment and donor CD45.2$^+$ cell engraftment within Mac1Gr1 (myeloid), B220 (B cell), and CD3 (T cell) populations in the BM of recipient CD45.1$^+$ mice 12 weeks following transplantation of BM cells from

irradiated *VE-cad-Cre;Ptn* $^{fl/fl}$ mice, control mice, or *LepR-Cre;Ptn* $^{fl/fl}$ mice. **p <0.01, ***p < 0.001, n = 20/group.

(C) Left: representative histograms show donor CD45.2$^+$ cell engraftment within BM LT-HSCs in recipient mice 12 weeks following transplantation of BM cells from irradiated *VE-cad-Cre;Ptn*$^{fl/fl}$ mice, control mice, or *LepR-Cre;Ptn*$^{fl/fl}$ mice. Right: mean donor CD45.2$^+$ cell engraftment in the LT-HSC population for each group. **p < 0.01, ***p < 0.001, n = 20/group.

(D) Representative flow cytometric analysis of donor CD45.2$^+$ cell engraftment in the BM of secondary recipient mice 12 weeks following transplantation of 3×10^6 BM cells collected from primary recipient mice in each group (represented in B) along with 2×10^5 CD45.1$^+$ competitor BM cells.

(E) Scatterplots showing the mean total donor CD45.2$^+$ cell engraftment and donor cell engraftment within BM myeloid, B cells, and T cells in secondary recipient mice in each group at 12 weeks. **p < 0.01, ***p < 0.001, n = 18–19/group;

Kruskal-Wallis test (one-way non-parametric ANOVA) with Dunn’s multiple comparisons test for all analyses. See also Figure S5.

KEY RESOURCES TABLE

REAGENT or RESOURCE	SOURCE	IDENTIFIER
Antibodies		
Anti-mouse VE-Cadherin	Biolegend	Cat. 138006; RRID:AB_10569114
Anti-LEPR / Leptin Receptor Antibody (aa956–986, PE), 200 μl	LifeSpan Biosciences, Inc (LSBio)	Cat. LS-C261834
Rabbit Anti-Leptin receptor Polyclonal Antibody, FITC	Bioss Antibodies	Cat. bs-0961R-FITC; RRID:AB_11074292
7-AAD Staining Solution (2 mL)	BD Biosciences	Cat. 559925
B220 (CD45R) APC-Cy7 Rat Anti-Mouse (0.1 mg)	BD Biosciences	Cat.552094; RRID:AB_394335
CD45 FITC Rat anti-Mouse (0.1 mg)	BD Biosciences	Cat.553079; RRID:AB_394609
CD45 PE Rat Anti-Mouse (0.1 mg)	BD Biosciences	Cat.553081; RRID:AB_394611
CD45.2 FITC Mouse anti-Mouse (0.5 mg)	BD Biosciences	Cat.553772; RRID:AB_395041
CD45.2 PE Mouse anti-Mouse (0.1 mg)	BD Biosciences	Cat.560695; RRID:AB_1727493
Gr-1 (Ly-6G and Ly-6C) PE Rat anti-Mouse (0.1 mg)	BD Biosciences	Cat.553128; RRID:AB_394644
Mac-1 (CD11b) PE Rat anti-Mouse (0.1 mg)	BD Biosciences	Cat.557397; RRID:AB_396680
Ter-119 APC Rat anti-Mouse (0.1 mg)	BD Biosciences	Cat.557909; RRID:AB_398635
V450 Rat Anti-Mouse CD3 Molecular Complex (50 μg)	BD Biosciences	Cat.561389; RRID:AB_10679120
V450 Rat IgG2b, κ Isotype Control (0.1 mg)	BD Biosciences	Cat.560457; RRID:AB_1645681
V450 Rat Anti-Mouse CD45 (50 μg)	BD Biosciences	Cat.560501; RRID:AB_1645275
Alexa Fluor 488 anti-mouse CD41 Antibody (100 μg)	Biolegend	Cat.133908; RRID:AB_10645332
CD150 Alexa Fluor 647 Rat anti-Mouse (50 μg)	BD Biosciences	Cat.562647
c-kit (CD117) PE Rat anti-Mouse (0.2 mg)	BD Biosciences	Cat.553355; RRID:AB_394806
Sca-1 (Ly-6A/E) APC-Cy7 Rat anti-Mouse (50 μg)	BD Biosciences	Cat.560654; RRID:AB_1727552
V450 Mouse Lineage Antibody Cocktail	BD Biosciences	Cat.561301; RRID:AB_10611731
APC FLK2^{+} (cd135)	BD Biosciences	Cat. 560718; RRID:AB_1727425
CD34 FITC	BD Biosciences	Cat.553733; RRID:AB_395017
APC Rat IgG2b, κ Isotype Control (0.1 mg)	BD Biosciences	Cat.556924; RRID:AB_10063104
APC-Cy7 Rat IgG2a, κ Isotype Control (0.1 mg)	BD Biosciences	Cat.552770; RRID:AB_394456
FITC Rat IgG1, κ Isotype Control (0.1 mg)	BD Biosciences	Cat.554684; RRID:AB_395508
FITC Rat IgG2a, κ Isotype Control (100 tests)	BD Biosciences	Cat.555843; RRID:AB_479727
PE Rat IgG2a, κ Isotype Control (0.1 mg)	BD Biosciences	Cat.553930; RRID:AB_479719

REAGENT or RESOURCE	SOURCE	IDENTIFIER
PE Rat IgG2b, κ Isotype Control (0.1 mg)	BD Biosciences	Cat.553989; RRID:AB_10049479
Alexa Fluor 647 IgG2a (0.1 mg)	BD Biosciences	Cat.557690; RRID:AB_396799
anti-GFP antibody	Aves	Cat. GFP-1020; RRID:AB_10000240
anti-chicken-DyLight-488 secondary	Thermo Fisher Scientific	Cat. SA5–10070; RRID:AB_2556650
Goat anti mouse osteopontin	R&D Systems	Cat. AF808; RRID:AB_2194992
CD31-Alexa-647	Biolegend	Cat. 102516; RRID:AB_2161029
mouse CD31 PE	R&D Systems	Cat. FAB3628G-100; RRID:AB_10972784
mouse endomucin AF750	Bioss Antibodies	Cat. bs-5884R-a750; RRID:AB_11090525
Anti-NG2 antibody [132.38] (ab50009) - 100ug	Abcam	Cat. ab50009; RRID:AB_881569
PDGFRa (CD140a) BV605	Biolegend	Cat. 135916; RRID:AB_2721548
PTPRZ1 AF647 antibody	Bioss Antibodies	Cat. bs-11327R-A647
Human/Mouse CXCL12/SDF-1 APC-conjugated Antibody	R&D	Cat. IC350A; RRID:AB_1964550
Perilipin Antibody AF647	R&D Systems	NB110–40760; RRID:AB_715043
Chemicals, Peptides, and Recombinant Proteins		
Liberase TL Research Grade	Sigma	Cat. 5401020001
Cal-Ex Decalcifier	Fisher Scientific	Cat. CS510–1D
Sucrose, BioUltra for molecular biology, ≥ 99.5% HPLC	Sigma-Aldrich	Cat. 84097–250 g
Gelatin (porcine skin)	Sigma-Aldrich	Cat. G1890–100G
Polyvinylpyrrolidone	Sigma-Aldrich	Cat. P5288–500G
Collagenase A	Sigma-Aldrich	Cat. 10103586001
DMEM-Ham F12	Thermo-Fisher	Cat. 21331–020
Fetal Bovine Serum	Thermo-Fisher	Cat. 16000044
Ascorbic Acid 2 Phosphate	Santa Cruz Biotechnology	Cat. sc-394304
L-glutamine	Thermo-Fisher	Cat. 25030081
Penicillin/Streptomycin	Thermo-Fisher	Cat. 10378016
IMDM	Thermo-Fisher	Cat. 12440061
Critical Commercial Assays		
Methocult GF M3434	STEMCELL Technologies	Cat. 03434
Miltenyi Lineage Cell Depletion kit	Miltenyi Biotec	Cat. 130–090-858
Taqman Gene Expression Master Mix	ThermoFisher	Cat. 4304437
High Capacity cDNA reverse transcription kit (1000 rxns)	LifeTech (supply center)	Cat. 4368813
Mouse PTN ELISA	Lifespan Biosciences	Cat. LS-F8143
Rneasy Micro Kit (50)	QIAGEN	Cat. 74004
Cytofix/Cytoperm buffer kit	BD Biosciences	Cat. 554714
Experimental Models: Organisms/Strains		
Mouse: C57/BL6	Jackson Laboratories	JAX: 000664

REAGENT or RESOURCE	SOURCE	IDENTIFIER
Mouse: B6.SJL	Jackson Laboratories	JAX: 002014
Mouse: PTN-EGFP	MMRC	MGI: 4847351
Mouse: PTN FL/FL	Duke Transgenic core	N/A
Mouse: Osteocalcin-Cre	Jackson Laboratories	JAX: 019509
Mouse: Leptin receptor-Cre	Jackson Laboratories	JAX: 008320
Mouse: VEcadherin-Cre	Jackson Laboratories	JAX: 006137
Mouse: Vav1-Cre	Jackson Laboratories	JAX: 008610
Mouse: Rosa25-TdTomato	Jackson Laboratories	JAX: 007914
Oligonucleotides		
mouse PTN Taqman gene expression assay	ThermoFisher	Mm01132688_m1
Mouse GAPDH primer Taqman gene expression assay	ThermoFisher	Mm99999915_g1
VECAD primer mouse (CDh5) Taqman gene expression assay	ThermoFisher	Mm00486938_m1
LepR primer mouse Taqman gene expression assay	ThermoFisher	Mm00486938_m1
ptn.S10:	IDT DNA	5’-TCT TGC TTT CAC AAC TCC AGT GTC-3’
ptn1.AS4	IDT DNA	5’-TCC ACA GCT GCC AAG ATG AAA ATC-3’.
Software and Algorithms		
FlowJo (v10)	TreeStar	https://www.flowjo.com/
GraphPad Prism 6.0	GraphPad Software	https://www.graphpad.com/
Just Another Colocalization Plugin (JACOP)	ImageJ	https://imagej.nih.gov/ij/
Maximum intensity projections	Leixa LAS X software	
AngioTool	https://ccrod.cancer.gov/confluence/display/ROB2/Downloads	Zudaire et al., 2011
Fiji	ImageJ	https://imagej.nih.gov/ij/
Huygens Professional Deconvolution Software	Scientific Volume Imaging	https://svi.nl/Huygens-Professional